"Monitoring the thermally induced transition from sp^3-hybridized into sp^2-hybridized carbons"

Dominique B. Schüpfer[a,*], Felix Badaczewski[b], Jan Peilstöcker[b], Juan Manuel Guerra-Castro[c], Hwirim Shim[d,e], Saleh Firoozabadi[f], Andreas Beyer[f], Kerstin Volz[f], Volker Presser[d,e], Christian Heiliger[c], Bernd Smarsly[b], Peter J. Klar[a]

[a] *Institute of Experimental Physics I and Center for Materials Research (LaMa), Justus Liebig University Giessen, 35392 Giessen, Germany*
[b] *Institute of Physical Chemistry and Center for Materials Research (LaMa), Justus Liebig University Giessen, 35392 Giessen, Germany*
[c] *Institute for Theoretical Physics and Center for Materials Research (LaMa), Justus Liebig University Giessen, 35392 Giessen, Germany*
[d] *INM - Leibniz Institute for New Materials, 66123 Saarbrücken, Germany*
[e] *Department of Materials Science and Engineering, Saarland University, 66123 Saarbrücken, Germany*
[f] *Department of Physics and Materials Science Center (WZMW), Philipps University Marburg, 35032 Marburg, Germany*

Figure S1 shows the wide-angle X-ray scattering data (WAXS) of the heat-treated nanodiamonds, which turn into carbon onions. Up to 1300 °C the diamond reflections are too strong to apply the model of Ruland and Smarsly to determine structural parameters such as the crystallite size L_a [1]. Samples prepared at temperatures in the range from 1700 °C and 2500 °C show non-graphitic structures and their WAXS data can be fitted (red line). At 3000 °C the sample is graphitic carbon and these kind of WAXS data can not be fitted due to the typical sharp reflections. For the diamond and graphite reflections the Scherrer's formula has to be used to estimate the crystallite size L_a [2].

*Corresponding author
Email address: dominique.b.schuepfer@exp1.physik.uni-giessen.de
(Dominique B. Schüpfer)

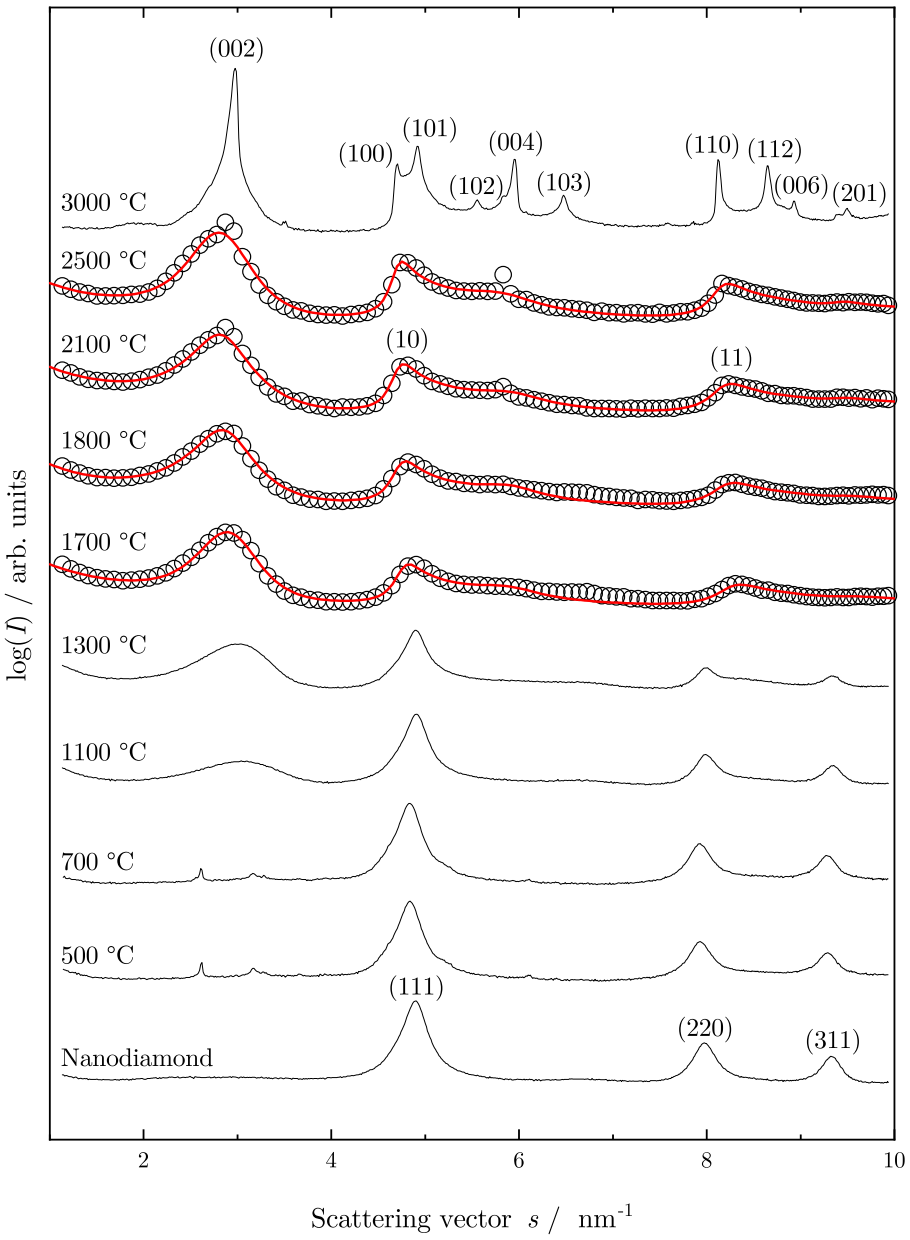

Figure 1: WAXS data of the heat-treated nanodiamonds, which turn into carbon onions. The red lines indicate the data fitting by the model of Ruland and Smarsly [1].

Figure S2 shows in the lower two graphs the series of Raman spectra of the nanodiamond-based samples prepared at different heat-treatment temperatures

taken with 325 nm excitation. The top two graphs show a Raman spectrum of the nanodiamond-based sample heat-treated at 3000 °C which was taken with 633 nm excitation for comparison. The graphs on the right zoom into the spectral region of the 2D band which can be used to distinguish between graphitic and non-graphitic carbon. The IUPAC defines non-graphitic (or turbostratic) carbon as stacks of graphene layers, which are rotated to each other and severely vary in their interlayer distances within one stack and therefore, show no order in the third dimension [3]. Because of the large distance between the graphene layers in non-graphitic carbon there is only a weak interaction between the sheets. Thus, the 2D Raman signal of non-graphitic carbon consists of one Raman band only and that of graphitic varbon consists of at least two overlapping bands. As a consequence, the 2D Raman signature is similar to that of graphene, i. e., the 2D Raman signal can be well described by one Lorentzian band. In contrast, the 2D Raman signal in graphitic carbon typically consists of two overlapping Lorentzian bands [4, 5, 6, 7, 8, 9]. In the figure, the 2D signal is observable only for the samples annealed at temperatures larger than 1800 °C. The signals reveal that these samples are mostly non-graphitic. It is worth noting, that the 2D Raman signal is shifted in frequency and more pronounced in case of an excitation wavelength in the visible range of the electromagnetic spectrum, e.g. 633 nm, than in case of an excitation in the ultraviolet range, e.g. 325 nm. The frequency shift arises because the 2D Raman process is a resonant process and involves the electronic states which are resonantly excited by the laser photons and their wavevectors q determine the region of the phonon dispersion contributing to the 2D signal. Different resonance profiles of G and 2D Raman process lead to the more pronounced 2D signal for visible excitation. Thus, distinguishing between non-graphitic and graphitic carbon based on the 2D signal is easier for 633 nm excitation. The top right graph of the figure shows the 2D Raman signal of the 3000 °C sample taken with 633 nm excitation. In the spectrum, a shoulder on the low-frequency side of the 2D Raman signal can be clearly discerned indicating the onset of graphitization.

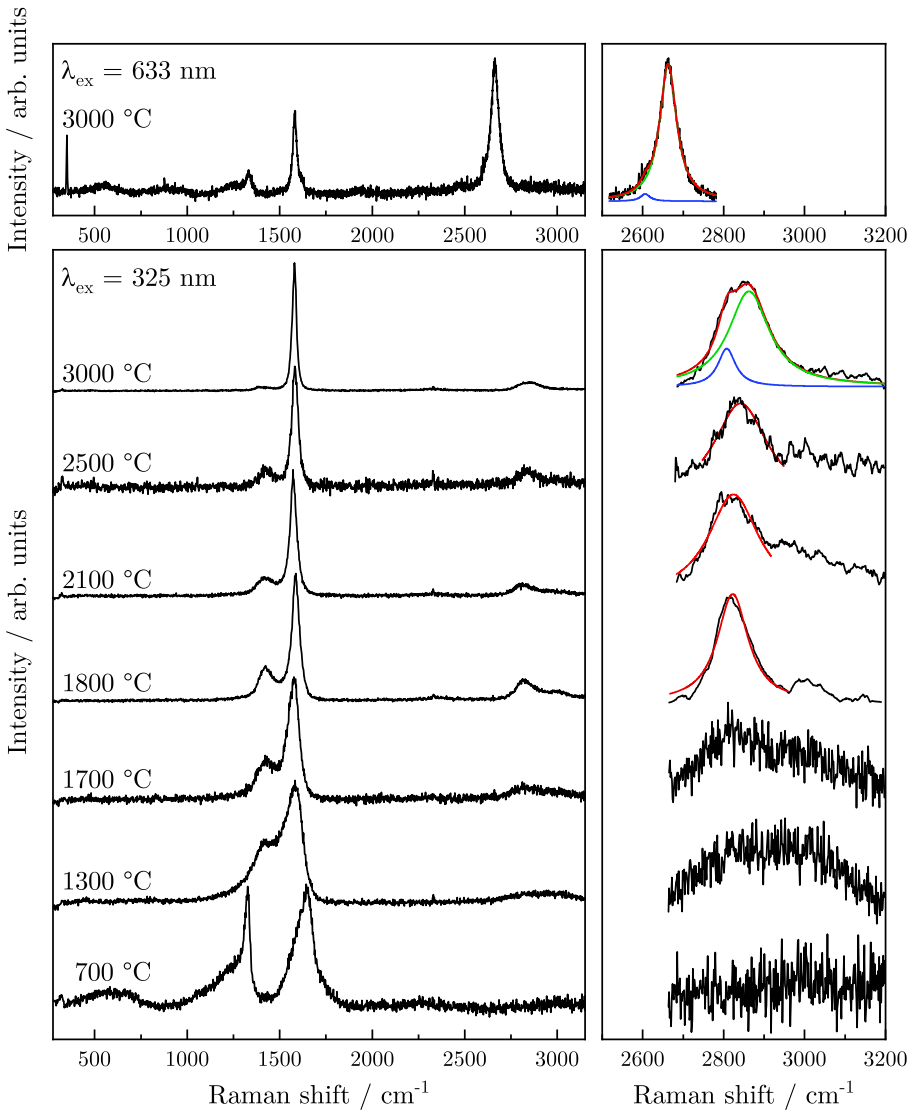

Figure 2: Top: Raman spectrum obtained with 633 nm excitation of the carbon sample derived from the nanodiamond-based presursor by heat treatment at 3000 °C. Bottom: Series of Raman spectra obtained with 325 nm excitation of carbon samples prepared from the nanodiamond-based presursor at different heat treatment temperatures between 700 °C and 3000 °C. The graphs on the right are magnifications of the spectra in the region of the 2D signal.

The band structure and the phonon dispersion of ideal graphene and di-

amond have been derived using density functional theory employing the software QUANTUM ESPRESSO [10, 11]. The atomic structure of graphene was relaxed and yielded lattice parameters in agreement with experiment within 0.01%. The electronic structure was computed using a non-relativistic and ultrasoft pseudo-potential within the Perdew-Burke-Ernzerhof parameterization of GGA for the exchange-correlation functional [12]. The phonon dispersions shown in Figure S3 were then calculated using the same input parameters, the same pseudo-potentials and the same exchange-correlation potentials as for the band structure calculation. The derived bandstructure and phonon dispersions served as input parameters for the Campbell-Fauchet modelling of the size dependence of the lineshape and positions of the G mode (at about $1580\,\mathrm{cm}^{-1}$) and optical mode (at about $1325\,\mathrm{cm}^{-1}$) of graphene and diamond, respectively, as well as for determining the size dependence of the lineshape and position of the D mode Raman signal of graphene (at about $1400\,\mathrm{cm}^{-1}$). Details can be found in [13, 14, 15]. We used the following dispersions $\omega(q)$ as input parameters for the Campbell-Fauchet modelling of the Raman signals in the two Raman processes involving the phonons close to the Γ-point of the Brillouin-zone where $q = 0$:

$$\begin{aligned} \omega^{\mathrm{opt}}_{\mathrm{graphene}}(q) &= 1558\,\mathrm{cm}^{-1} \\ \omega^{\mathrm{opt}}_{\mathrm{diamond}}(q) &= 1332\,\mathrm{cm}^{-1} \end{aligned}$$

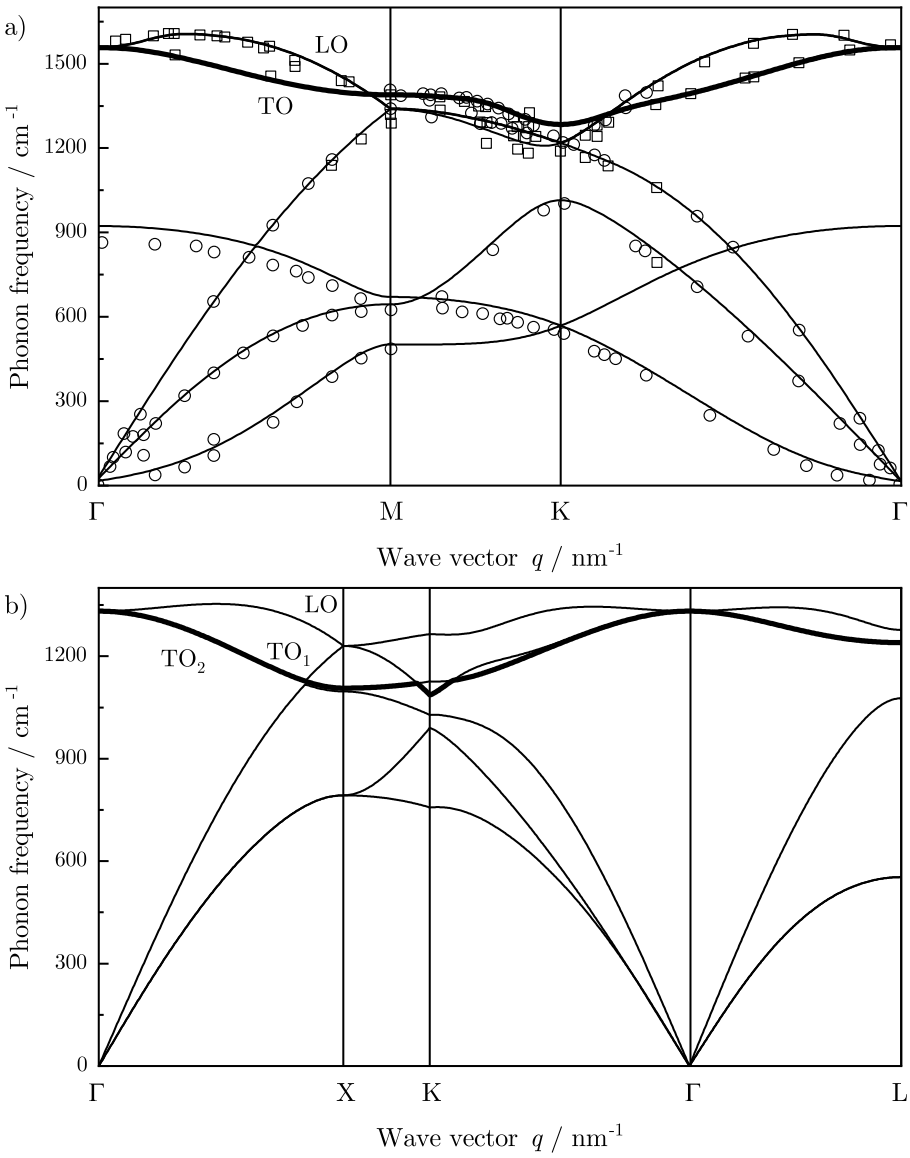

Figure 3: a) Phonon dispersion of graphene. b) Phonon dispersion of diamond calculated by density functional theory.

Figure S4 shows a comparison of the Raman spectra of the adamantane-based carbon sample heat-treated at 525 °C obtained with 325 nm and 785 nm excitation with Raman spectra of various molecules obtained using 325 nm ex-

citation. The adamantane-based carbon sample shows broad Raman signals (black solid lines). These signals are likely to consist of contributions of a large variety Raman signals from molecules forming during the transformation process into sp^2-bonded carbon material. Exemplarily, we show Raman spectra of molecules which possess only sp^1, sp^2 or sp^3-hybridized bonds between their carbon atoms. In figure 4a) coronene and pyrene represent the class of sp^2-bonded molecules (red), higher diamondoids like triamantane and two adamantane cages coupled by an ethylene bridge represent sp^3-bonded molecules (blue) and polyethylene is chosen to represent chainlike sp^1-bonded species (green). In addition, the superposition of all these molecular spectra is shown to illustrate the similarity of the corresponding envelope curve with the broad bands in the spectrum of the adamantane-based carbon sample heat-treated at 525 °C.

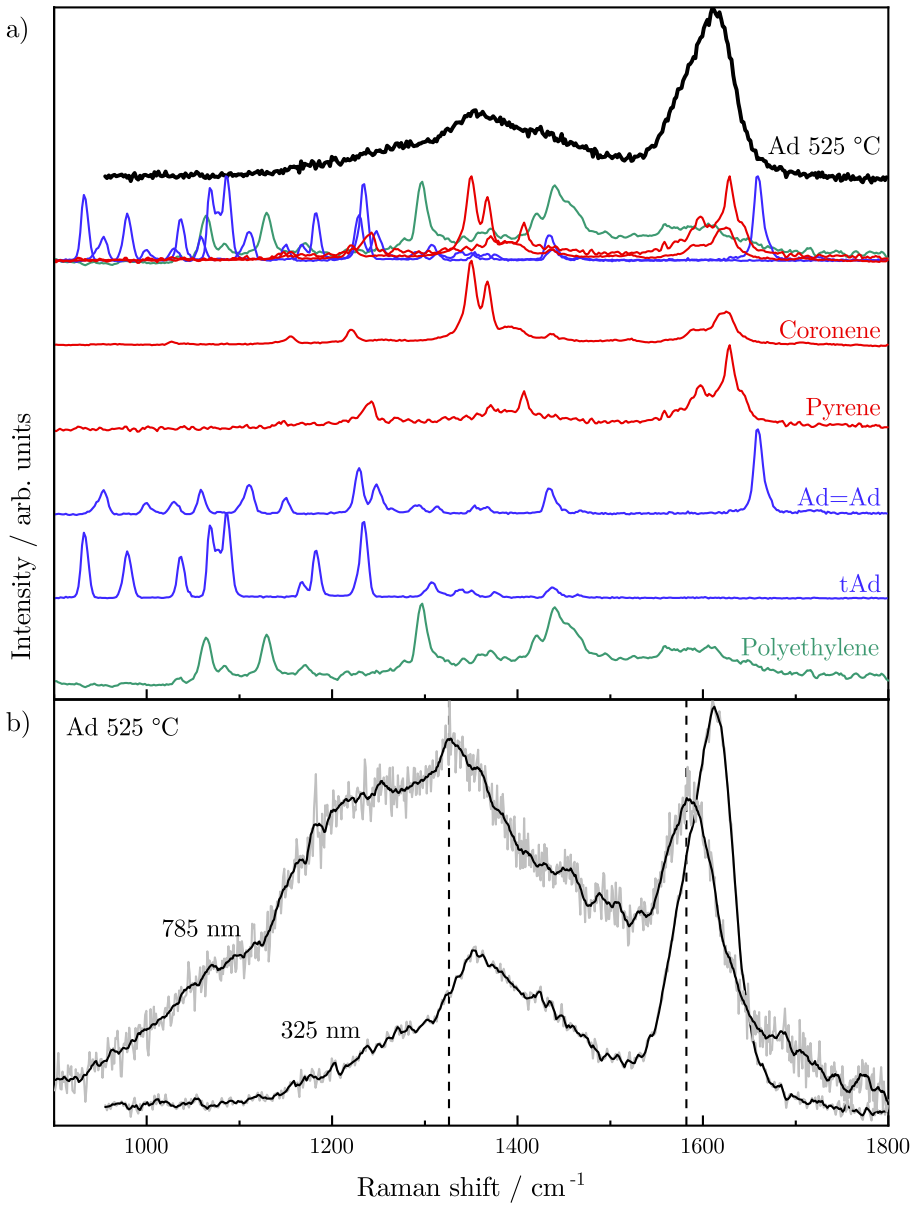

Figure 4: a) Comparison of the Raman spectrum of an adamantane-based carbon sample heat-treated at 525 °C with Raman data of the sp^2-hybridized molecules coronene and pyrene (red lines), of sp^3-bonded triamantane and two coupled adamantene cages (via an ethylene bridge) Ad=Ad (blue lines) and of sp^1-bonded polyethylene (green line). A superposition of all these molecular Raman spectra already resembles the Raman spectrum of adamantane-based carbon heat-treated at 525 °C quite well. All spectra are taken with an excitation wavelength of 325 nm. b) Raman spectra of the adamantane-based samples heat-treated at 525 °C for two different excitation wavelengths, i.e., of 325 nm and 785 nm.

Figure S4b) is a comparison of Raman spectra of the same adamantane-based carbon sample heat-treated at 525 °C obtained with two different excitaion wavelengths. The different weights of the spectral features in the two spectra arise due to different resonance profiles of the Raman signals corresponding to molecules of different size and bond configuration. When the excitation wavelength is varied, HOMO-LUMO gaps of different molecular species are in resonance. For example, in case of sp^2-bonded molecules the optical gap decreases with increasing size of the molecules or crystallites [16]. The same holds for sp^3-bonded species. This strongly contributes to the dependence of the intensity ratio I_D/I_G [17, 18] and the position of the D band on excitation wavelength. In the 785 nm spectrum, the left side of the D band is strongly enhanced compared to the 325 nm spectrum. This might be due to the second A_{1g} band at around 1250 cm^{-1}, which is typical for larger polycyclic aromatic hydrocarbons (PAHs) such as coronene [19, 20] or due to a resonance of the Raman signals of sp^3-bonded molecules. A comparison of the two Raman spectra of this carbon sample with the the Raman band positions and the intensity ratio of D and G band of the pitch and resin-based carbon samples of known lateral size suggests the existence of crystallites with a sizes up to 1.5 nm.

References

[1] Ruland W, Smarsly B. X-ray scattering of non-graphitic carbon: an improved method of evaluation. J Appl Cryst 2002;35:624–33. doi:10.1107/S0021889802011007.

[2] Scherrer P. Bestimmung der größe und der inneren struktur von kolloidteilchen mittels röntgenstrahlen. Nachrichten von der Gesellschaft der Wissenschaften zu Göttingen, Mathematisch-Physikalische Klasse 1918;1918:98.

[3] Fitzer E, Köchling KH, Boehm HP, Marsh H. Recommended terminology for the description of carbon as a solid. Pure Appl Chem 1995;67(3):473–506. doi:10.1351/pac199567030473.

[4] Jorio A, Saito R, Dresselhaus G, Dresselhaus MS. Raman spectroscopy in graphene related systems. WILEY-VCH Verlag GmbH & Co. KGaA; 2011. ISBN 978-3-527-40811-5.

[5] Malard LM, Pimenta MA, Dresselhaus G, Dresselhaus MS. Raman spectroscopy in graphene. Phy Rep 2009;473(5-6):51–87. doi:10.1016/j.physrep.2009.02.003.

[6] Cançado LG, Pimenta MA, Saito R, Jorio A, Ladeira LO, Grueneis A, et al. Stokes and anti-stokes double resonance raman scattering in two-dimensional graphite. Phys Rev B 2002;66(3):035415. doi:10.1103/PhysRevB.66.035415.

[7] Cançado L, Takai K, Enoki T, Endo M, Kim Y, Mizusaki H, et al. Measuring the degree of stacking order in graphiteby raman spectroscopy. Carbon 2008;46(2):272–5. doi:10.1016/j.carbon.2007.11.015.

[8] Cançado LG, Reina A, Kong J, Dresselhaus MS. Geometrical approach for the study of g' band in the raman spectrum of monolayer graphene, bilayer graphene, and bulk graphite. Phys Rev B 2008;77(24):245408. doi:10.1103/PhysRevB.77.245408.

[9] Ferrari AC, Meyer JC, Scardaci V, Casiraghi C, Lazzeri M, Mauri F, et al. The Raman fingerprint of graphene. Phys Rev Lett 2006;97:187401. doi:10.1103/PhysRevLett.97.187401.

[10] Giannozzi P, Baroni S, Bonini N, Calandra M, Car R, Cavazzoni C, et al. QUANTUM ESPRESSO: a modular and open-source software project for quantum simulations of materials. J Phys: Condens Matter 2009;21(39):395502. doi:10.1088/0953-8984/21/39/395502.

[11] Giannozzi P, Andreussi O, Brumme T, Bunau O, Nardelli MB, Calandra M, et al. Advanced capabilities for materials modelling with quantum ESPRESSO. J Phys: Condens Matter 2017;29(46):465901. doi:10.1088/1361-648X/aa8f79.

[12] Perdew JP, Burke K, Ernzerhof M. Generalized gradient approximation made simple. Phys Rev Lett 1996;77(18):3865–8. doi:10.1103/PhysRevLett.77.3865.

[13] Schüpfer DB, Badaczewski F, Guerra-Castro JM, Hofmann DM, Heiliger C, Smarsly B. Assessing the structural properties of graphitic and non-graphitic carbons by raman spectroscopy. Carbon 2020;161:359–72. doi:10.1016/j.carbon.2019.12.094.

[14] Campbell IH, Fauchet PM. The effects of microcrystal size and shape on the one phonon Raman spectra of crystalline semiconductors. Solid State Commun 1986;58(10):739–41. doi:10.1016/0038-1098(86)90513-2.

[15] Fauchet PM, Campbell IH. Raman spectroscopy of low-dimensional semiconductors. Crit Rev Solid State 1988;14(sup1):s79–101. doi:10.1080/10408438808244783.

[16] Müller S, Müllen K. Expanding benzene to giant graphenes: towards molecular devices. Phil Trans R Soc A 2007;365:1453–72. doi:10.1098/rsta.2007.2026.

[17] Cançado LG, Jorio A, Ferreira EHM, Stavale F, Achete CA, Capaz RB, et al. Quantifying defects in graphene via Raman spectroscopy at different excitation energies. Nano Lett 2011;11(8):3190. doi:10.1021/nl201432g.

[18] Ferrari AC, Robertson J. Resonant Raman spectroscopy of disordered, amorphous, and diamondlike carbon. Phys Rev B 2001;64:075414. doi:10.1103/PhysRevB.64.075414.

[19] Castiglioni C, Negri F, Rigolio M, Zerbi G. Raman activation in disordered graphites of the a_1 symmetry forbidden $k \neq 0$ phonon: The origin of the D line. J Chem Phys 2001;115(8):3769–78. doi:10.1063/1.1381529.

[20] Castiglioni C, Mapelli C, Negri F, Zerbi G. Origin of the D line in the Raman spectrum of graphite: A study based on Raman frequencies and

intensities of polycyclic aromatic hydrocarbon molecules. J Chem Phys 2001;114(2):963–74. doi:10.1063/1.1329670.